Geology

Isotopic evidence for changes in the zinc cycle during Oceanic Anoxic Event 2 (Late Cretaceous)

--Manuscript Draft--

Manuscript Number:	G40226R1
Full Title:	Isotopic evidence for changes in the zinc cycle during Oceanic Anoxic Event 2 (Late Cretaceous)
Short Title:	Isotopic evidence for changes in the zinc cycle during Oceanic Anoxic Event 2
Article Type:	Article
Keywords:	zinc isotopes; OAE 2; Cenomanian-Turonian; anoxia; nutrients
Corresponding Author:	Tim Sweere University of Oxford Oxford, Oxfordshire UNITED KINGDOM
Corresponding Author Secondary Information:	
Corresponding Author's Institution:	University of Oxford
Corresponding Author's Secondary Institution:	
First Author:	Tim Sweere
First Author Secondary Information:	
Order of Authors:	Tim Sweere
	Alexander J. Dickson
	Hugh C. Jenkyns
	Don Porcelli
	Maya Elrick
	Sander H.J.M. van den Boorn
	Gideon M. Henderson
Order of Authors Secondary Information:	
Manuscript Region of Origin:	UNITED KINGDOM
Abstract:	Widespread deposition of organic-rich shales during the Late Cretaceous Oceanic Anoxic Event 2 (OAE 2, ~94 Ma) occurred during a period of significant global palaeoenvironmental and geochemical change. It has been proposed that an increase in nutrient input to the ocean during OAE 2 was the key mechanism that generated and sustained high rates of organic-matter burial over timescales of 103-105 years. Zn is a bio-essential micronutrient and the proportion of Zn burial in oxic sediments relative to burial in organic-rich continental margin sediments is reflected in its seawater isotope composition. The first Zn-isotope records dating from the Cretaceous are presented here from three coeval carbonate successions: two from Europe (southern England and southern Italy) and one from Central America (southern Mexico). The new data show reproducible stratigraphic Zn-isotope patterns in spatially and lithologically diverse carbonate successions. Excursions to lower Zn-isotope values may be linked to the input of magmatic zinc, changes in the proportion of Zn burial into organic-rich sediments, and the liberation of previously buried Zn during an episode of widespread seafloor re-oxygenation during OAE 2 (the Plenus Cold Event).

Publisher: GSA
Journal: GEOL: Geology
DOI:10.1130/G40226.1

Isotopic evidence for changes in the zinc cycle during Oceanic Anoxic Event 2 (Late Cretaceous)

Tim C. Sweere[1], Alexander J. Dickson[1], Hugh C. Jenkyns[1], Don Porcelli[1], Maya Elrick[2], Sander H.J.M. van den Boorn[3], and Gideon M. Henderson[1]

[1]*Department of Earth Sciences, University of Oxford, South Parks Road, Oxford OX1 3AN, UK*

[2]Department of Earth and Planetary Sciences, MSCO3-2040, 1 University of New Mexico, Albuquerque, New Mexico 87131, USA

[3]*Shell Projects and Technology, Kessler Park, 2288 GS Rijswijk, Netherlands*

ABSTRACT

Widespread deposition of organic-rich shales during the Late Cretaceous Oceanic Anoxic Event 2 (OAE 2, ~94 Ma) occurred during a period of significant global palaeoenvironmental and geochemical change. It has been proposed that an increase in nutrient input to the ocean during OAE 2 was the key mechanism that generated and sustained high rates of organic-matter burial over timescales of 10^3–10^5 years. Zn is a bio-essential micronutrient and the proportion of Zn burial in oxic sediments relative to burial in organic-rich continental margin sediments is reflected in its seawater isotope composition. The first Zn-isotope records dating from the Cretaceous are presented here from three coeval carbonate successions: two from Europe (southern England and southern Italy) and one from Central America (southern Mexico). The new data show reproducible stratigraphic Zn-isotope patterns in spatially and lithologically diverse carbonate successions. Excursions to lower Zn-isotope values may be linked to the input

of magmatic zinc, changes in the proportion of Zn burial into organic-rich sediments, and the liberation of previously buried Zn during an episode of widespread seafloor re-oxygenation during OAE 2 (the Plenus Cold Event).

INTRODUCTION

Several distinct intervals of widespread deposition of organic-rich black shales occurred during some of the most extreme perturbations to global climate and oceanography of the Phanerozoic Eon. Mesozoic Oceanic Anoxic Events (OAEs) have been associated with rapid warming, the spread of low-oxygen marine environments and perturbations to floral and faunal diversity and biogeochemical cycles (e.g., Jenkyns, 2010).

For the Late Cretaceous OAE 2 (Cenomanian–Turonian, ~94 Ma), geochemical models indicate that the initiation and maintenance of high rates of organic-matter production required an increase in oceanic nutrient inventories (Monteiro et al., 2012). Indeed, proxy evidence suggests that widespread volcanism may have caused an increased supply of nutrients to the ocean, either through basalt–seawater interaction, or indirectly by warming-induced intensification of (silicate) weathering of mafic and felsic rocks and by an intensified hydrological cycle (e.g., Turgeon and Creaser, 2008; Jenkyns et al., 2017). Although these observations constitute evidence for potential changes in nutrient inventories, direct evidence for the availability of bio-limiting nutrients in the oceans is currently limited, largely due to a lack of applicable proxies.

The major nutrients phosphorus and nitrogen may have been relatively abundant due to regeneration of the former from anoxic sediments (Mort et al. 2007 and references therein) and increased fixation of the latter by abundant diazotrophic cyanobacteria

utilizing atmospheric di-nitrogen in nitrate-depleted seawater (Kuypers et al., 2004). Extensive burial of organic matter during OAEs may have triggered a biotic response as redox-sensitive bio-limiting metals were removed from global seawater (e.g., Owens et al., 2016). Assessing the importance of feedback mechanisms between trace-metal availability, biotic response, and the carbon cycle requires the use of appropriate proxies. During times of major global change, such as the OAEs, proxies that enable reconstruction of ocean chemistry at a regional or global scale are particularly valuable.

Zn-Isotope Systematics

Although not limiting to overall productivity in the modern ocean, Zn is fundamental for many life processes and its concentration is reduced to near zero by biological activity in the surface ocean (e.g., Wyatt et al. 2014). Zn has a present-day oceanic residence time of ~11,000 years (Little et al., 2014). The Zn-isotope composition of today's deep ocean is homogeneous ($\delta^{66}Zn$ = ~0.5 ‰ ± 0.14; 2 SD, Conway and John, 2014) and is isotopically heavier than the bulk silicate Earth and sources of Zn to the ocean such as rivers, dust, hydrothermal springs, and benthic inputs (Little et al., 2014; Vance et al., 2016 and references therein). Reported oxic sinks of Zn (e.g., Fe-Mn oxyhydroxides) are isotopically heavier than inputs and deep-ocean values ($\delta^{66}Zn$>~0.5) (e.g., Little et al., 2014). Organic-rich continental-margin sediments are so far the only documented removal sink of isotopically light Zn from the oceans (Little et al., 2016). The low $\delta^{66}Zn$ values observed for these sediments may be the result of non-quantitative removal of Zn in sulfides, or due to scavenging of isotopically heavy Zn just below the surface ocean, resulting in low $\delta^{66}Zn$ values in the photic zone where organic material is generated (Little et al., 2016; Vance et al., 2016; John et al., 2017).

Publisher: GSA
Journal: GEOL: Geology
DOI:10.1130/G40226.1

Alteration of the input and output fluxes of Zn to and from the ocean in concert with global environmental changes might thus be expected to have impacted the marine cycling of Zn. A relative increase in the removal flux of Zn from seawater into organic-rich continental margin sediments compared to Zn burial in oxic sediments would cause a shift toward higher δ^{66}Zn values in the global ocean and *vice versa*; a relative increase in the input of isotopically light Zn from hydrothermal sources or remobilized from margin sediments can result in lower δ^{66}Zn values in the global ocean (Fig. 1).

Modern surface-ocean δ^{66}Zn values are generally lower than the deep ocean by ~0.5‰, but show a high degree of spatial variability (δ^{66}Zn = –1.1 to +0.9‰, Conway and John, 2014). These variations are likely caused by biological uptake of Zn, scavenging of isotopically heavy Zn, and the lateral or vertical advection of water masses (e.g. Conway and John, 2014). Pelagic and shallow-water carbonates have previously been used to reconstruct upper-ocean Zn-isotope compositions for intervals of Quaternary, Neoproterozoic, and Late Permian–Early Triassic time (Pichat et al., 2003; Kunzmann et al., 2013; Liu et al., 2017). The use of such deposits as archives for past global seawater chemistry requires consideration of Zn-isotope effects caused by the balance of inputs and outputs to the local upper ocean, superimposed on slower changes in the global mass balance of Zn that might lead to changes in homogenous deep-water composition.

MATERIAL AND METHODS

Data are presented for three marine carbonate successions that span the Cenomanian–Turonian boundary interval: the nannofossil-rich English chalk exposed near Eastbourne, southern England; shallow-water platform carbonates exposed near Raia

del Pedale, Southern Apennines, Italy; and the Barranca el Cañón limestone section in the state of Guerrero, southern Mexico (Fig. 2). The Eastbourne chalk, comprising coccoliths, planktonic foraminifera and some macrofossils, formed primarily in the photic zone, and was deposited in waters that were probably no deeper than 600m (Hancock, 1975). The platform carbonates found at the other two locations were primarily formed from skeletal material in shallower (i.e., a few tens of meters or less) waters (Parente et al., 2008; Elrick et al., 2009). The well-studied Eastbourne sample set is used as the primary data set here because it has a stratigraphically expanded and well-documented OAE 2 succession, containing sediments with little diagenetic alteration and relatively low amounts of detrital and/or organic matter (TOC < 0.26 wt.%) (Hancock, 1975; Tsikos et al., 2004). The other two outcrops have well-established carbon-isotope and/or bio-stratigraphic profiles that allow direct comparison with the Eastbourne succession, but may have been compromised as geochemical archives due to their more variable original carbonate mineralogy (aragonite and calcite) and greater degree of lithification (Parente et al., 2008; Elrick et al., 2009, SI).

Zn-isotope data were measured relative to the IRMM 3702 standard on carbonates that were selectively leached from bulk rocks and reported as $\delta^{66}Zn$ after adding +0.28% to allow direct comparison with previously published data ($\delta^{66}Zn_{JMC\text{-}Lyon}$). Further analytical details are provided in the Supplementary Information (SI).

RESULTS

$\delta^{66}Zn$ values average 1.06 ± 0.38 ‰ (2 s.d., n = 28), 1.14 ± 0.51 ‰ (2 s.d., n = 22), and 0.89 ± 0.49 ‰ (2 s.d., n = 14) for the Eastbourne, Raia del Pedale and Barranca el Cańón data sets respectively (Fig. 3), and are comparable to data from other

palaeoenvironmental studies on biogenic carbonates (~0.91‰, Pichat et al., 2003; ~0.75‰, Liu et al., 2017). The most striking features of the primary Eastbourne data are two ~0.5‰ shifts toward lower δ^{66}Zn values, marked 'A' and 'B' in Figure 3, separated by an increase toward higher values. A similar shift to lower δ^{66}Zn values is also seen in the Raia del Pedale data at Event B. Isotope data from Barranca el Cańón are too sparse and scattered to resolve clear trends, despite their rather similar average values to those at other sites. Events A and B in δ^{66}Zn correspond with recognized features of the δ^{13}C stratigraphy of OAE 2 (Tsikos et al., 2004), namely the first increase in δ^{13}C at the onset of OAE 2 (which occurs after the start of Event A) and the decrease in δ^{13}C that corresponds with the Plenus Cold Event (Event B).

Zn/Ca values average 15 ± 21 (2 s.d., n = 48), 3.6 ± 7.1 (2 s.d., n = 21), and 14 ± 38 (2 s.d., n = 46) μmol/mol for the Eastbourne, Raia del Pedale and Barranca el Cańón data sets respectively (Fig. 3), and are comparable to the range in Zn/Ca observed in marine calcifiers (e.g., Zn/Ca in benthic foraminifera: ~3.3 μmol/mol, Marchitto et al., 2000; planktonic foraminifera: ~35 μmol/mol, Boyle, 1981). Marked stratigraphic features in Zn/Ca include an increase in Zn/Ca in Eastbourne during Event B and increases in Barranca el Cańón during Event B and the Early Turonian.

Al and Mn abundances in the leachates are used to assess the leaching of clays and ferromanganese coatings for the Eastbourne and Barranca el Cańón sample sets. These data suggest that stratigraphic trends in Zn/Ca and δ^{66}Zn are not the result of leaching of Zn from clays or ferromanganese coatings, as no significant change in Al or Mn content is associated with changes in δ^{66}Zn (see SI).

DISCUSSION

Publisher: GSA
Journal: GEOL: Geology
DOI:10.1130/G40226.1

Carbonates as an Archive for $\delta^{66}Zn$

Differences between $\delta^{66}Zn$ observed in this study, other carbonate studies, and the modern ocean might reflect changes in the $\delta^{66}Zn$ value of the global oceans through time. However, interpretation is not straightforward because carbonate sediments are likely to record shallow-water seawater compositions, which can vary significantly relative to the deep ocean composition. Carbonate $\delta^{66}Zn$ values that are considerably higher than modern deep-waters (0.5‰) are also difficult to explain, because surface seawater (0–1000m) generally has lower $\delta^{66}Zn$ than deep-water. This difference may suggest a significant systematic isotope fractionation (>+0.4‰) during incorporation of Zn into marine carbonates or adsorbed to calcite surfaces, as has been suggested by Dong and Wasylenki (2016). Rather than seeking to quantify this offset more precisely, we focus on relative changes in the $\delta^{66}Zn$ values within our records.

Surface-Ocean Processes and Spatial Patterns

For large parts of the Cenomanian–Turonian interval, $\delta^{66}Zn$ values between the three sites are similar, which is surprising considering the heterogeneity of dissolved $\delta^{66}Zn$ in the modern surface ocean. During such intervals, the fraction of Zn removed from the surface ocean must be similar at the three sites. Common stratigraphic variations in $\delta^{66}Zn$ (i.e., Event B), which approach amplitudes of ~0.5 ‰, might possibly have been caused by near-synchronous changes in the expression of local processes on upper-ocean Zn cycling at each location (e.g., a change in the removal rate from near-surface waters by biological fixation or adsorption). However, such a process seems unlikely considering the different Zn/Ca patterns between the cores during this time interval. Whereas the upper part of the Event B record at Eastbourne is associated with higher Zn

abundances, values at Raia del Pedale are relatively constant, excluding the notion of local upper-ocean Zn-inventory changes as a likely explanation for the observed δ^{66}Zn values at both sites. Hence, the common Zn-isotope stratigraphic fluctuations at Eastbourne and Raia del Pedale more plausibly record changes in the whole-ocean isotopic composition of Zn, and thus represent changes in its global cycling during OAE 2.

Zn-Cycle Perturbation in Relation to a Magmatic Episode—Event A

Osmium-isotope data suggest that increased basalt-seawater interaction persisted throughout much of the OAE 2 (Turgeon and Creaser, 2008; Du Vivier et al., 2015), a phenomenon that likely favored the elevated input of dissolved trace metals into the ocean (e.g., Elrick et al., 2009). The initial shift of Os isotopes to unradiogenic values, like that of δ^{66}Zn, pre-dates the onset of the positive carbon-isotope excursion, conventionally taken to record the beginning of OAE 2. This shift in Os isotopes has been related to the input of unradiogenic Os from volcanism or some other form of basalt–seawater interaction involving one or more Large Igneous Provinces (Turgeon and Creaser, 2008; Du Vivier et al., 2015; Jenkyns et al., 2017).

The first drop in δ^{66}Zn (Event A, Fig. 3) may represent a particularly strong pulse of isotopically light Zn to the ocean from hydrothermal fluids or low-temperature reactions between seawater and mafic rocks (cf, Liu et al., 2017). A rapid Zn input from this source may have created heterogeneities in the isotopic composition of surface waters, which could explain the variable magnitude of the negative Zn-isotope excursions at Raia del Pedale and Eastbourne. This observation would directly link the onset of a magmatic episode with ocean nutrification as a trigger for increased carbon burial during

Publisher: GSA
Journal: GEOL: Geology
DOI:10.1130/G40226.1

the initial phase of OAE 2. Increased Zn burial into globally expanding organic-rich sediments shortly after Event A (and the initial unradiogenic Os-isotope shift), can explain the pattern of gradually increasing Zn-isotope compositions, despite consistently unradiogenic osmium-isotope seawater values during this interval.

Zinc-Cycle Perturbation during the Plenus Cold Event—Event B

The second drop toward lower δ^{66}Zn values (Event B, Fig. 3) occurred during the Plenus Cold Event, which was associated with re-oxygenation in many locations and had a major effect on ocean chemistry (Jenkyns et al., 2017; Clarkson et al., 2018). A relative decrease in the size of organic-rich continental margin sinks for isotopically light Zn as a result of improved bottom-water oxygenation explains lower δ^{66}Zn values observed at both Eastbourne and Raia del Pedale. An additional factor driving the observed Zn-isotope variations during the Plenus Cold Event and the elevated Zn/Ca ratios in Eastbourne during this time interval may have been the release of isotopically light Zn from organic-rich continental-margin sediments as a result of an increase in (aerobic) biodegradation of organic matter and sulphides, as observed in parts of the modern ocean (Conway and John, 2014). Elevated concentrations of conservative redox-sensitive trace metals (e.g., Mo, U) observed previously at both Eastbourne and Raia del Pedale have been linked to the re-oxidation of previously buried organic-rich sediments (Jenkyns et al., 2017). By contrast, the absence of elevated Zn/Ca ratios at Raia del Pedale (Fig. 3) is probably due to the very shallow (less than a few tens of meters) setting of this site and the high efficiency of Zn removal that is likely to have occurred from surface waters in extremely oligotrophic conditions.

The Plenus Cold Event has been associated with biotic turnover and changes in the distribution of phytoplankton (Parente et al., 2008; Van Helmond et al., 2016 and references therein). The new Zn-isotope data suggest that, in addition to oxygenation and cooling, perturbations to micronutrient cycles might have played a role in driving these paleoecological changes. A perturbation to the Zn cycle during the Plenus Cold Event, as inferred from relatively light Zn-isotope compositions and elevated Zn/Ca ratios in Eastbourne and Barranca el Cańón, can be directly correlated with the extinction of larger benthic foraminifera, as recorded in the Southern Apennines of Italy. These K-strategists were adapted to nutrient-poor conditions and therefore suffered from the switch to more nutrient-rich conditions during the Plenus Cold Event (Parente et al., 2008). Surface-ocean nutrification during the Plenus Cold Event was inferred previously from the distribution of foraminifera alone. The data presented here support this model of a perturbation to the (micro)nutrient cycle.

CONCLUSIONS

Zn-isotope trends in marine carbonates from England, Italy and Mexico demonstrate perturbations to the zinc cycle during the Cenomanian–Turonian interval, with isotopically light Zn-isotope compositions observed just prior to the onset of OAE 2 and during the Plenus Cold Event. This work constitutes the first isotopic evidence for changes in the Zn cycle during the Cretaceous and supports the hypothesis that ocean nutrification was important in driving widespread and intense organic-carbon burial at the onset of OAE 2. Specifically, the correlation between Zn-isotope variations and the extinction of benthic foraminifera recorded in platform carbonates of the Southern Apennines is consistent with a link between the abundance of micronutrients and the

extinction of marine fauna adapted to oligo- and mesotrophic conditions. Given the reproducibility of stratigraphic Zn-isotope patterns in spatially and lithologically diverse carbonate successions, this proxy may be an important tool for reconstructing the ocean redox and nutrient chemistry in ancient oceans.

ACKNOWLEDGMENTS

We gratefully acknowledge Shell for research funding and Seth John and two anonymous reviewers for thoughtful comments.

REFERENCES CITED

Boyle, E.A., 1981, Cadmium, zinc, copper, and barium in foraminifera tests: Earth and Planetary Science Letters, v. 53, p. 11–35, https://doi.org/10.1016/0012-821X(81)90022-4.

Conway, T.M., and John, S.G., 2014, The biogeochemical cycling of zinc and zinc isotopes in the North Atlantic Ocean: Global Biogeochemical Cycles, v. 28, p. 1111–1128, https://doi.org/10.1002/2014GB004862.

Clarkson, M.O., Stirling, C.H., Jenkyns, H.C., Dickson, A.J., Porcelli, D., Moy, C.M., Pogge von Strandmann, P.A.E., Cooke, I.R., and Lenton, T.M., 2018, Uranium isotope evidence for two episodes of deoxygenation during Oceanic Anoxic Event 2: Proceedings of the National Academy of Sciences of the United States of America, (in press).

Dong, S., and Wasylenki, L.E., 2016, Zinc isotope fractionation during adsorption to calcite at high and low ionic strength: Chemical Geology, v. 447, p. 70–78, https://doi.org/10.1016/j.chemgeo.2016.10.031.

Du Vivier, A., Selby, D., Condon, D., Takashima, R., and Nishi, H., 2015, Pacific $^{187}Os/^{188}Os$ isotope chemistry and U–Pb geochronology: Synchroneity of global Os isotope change across OAE 2: Earth and Planetary Science Letters, v. 428, p. 204–216, https://doi.org/10.1016/j.epsl.2015.07.020.

Elrick, M., Molina-Garza, R., Duncan, R., and Snow, L., 2009, C-isotope stratigraphy and paleoenvironmental changes across OAE2 (mid-Cretaceous) from shallow-water platform carbonates of southern Mexico: Earth and Planetary Science Letters, v. 277, p. 295–306, https://doi.org/10.1016/j.epsl.2008.10.020.

Hancock, J.M., 1975, The petrology of the Chalk: Proceedings of the Geologists' Association, v. 86, p. 499–535.

Jenkyns, H. C., 2010, Geochemistry of oceanic anoxic events: Geochemistry, Geophysics, Geosystems, v. 11, Q03004, doi:20.1029/2009GC002788.

Jenkyns, H.C., Dickson, A.J., Ruhl, M., and Van Den Boorn, S.H., 2017, Basalt–seawater interaction, the Plenus Cold Event, enhanced weathering and geochemical change: Deconstructing Oceanic Anoxic Event 2 (Cenomanian–Turonian, Late Cretaceous): Sedimentology, v. 64, p. 16–43, https://doi.org/10.1111/sed.12305.

John, S.G., Kunzmann, M., Townsend, E.J., and Rosenber, A.D., 2017, Zinc and cadmium stable isotopes in the geological record: A case study from the post-snowball Earth Nuccaleena cap dolostone: Palaeogeography, Palaeoclimatology, Palaeoecology, v. 466, p. 202–208, https://doi.org/10.1016/j.palaeo.2016.11.003.

Kunzmann, M., Halverson, G.P., Sossi, P.A., Raub, T.D., Payne, J.L., and Kirby, J., 2013, Zn isotope evidence for immediate resumption of primary productivity after snowball Earth: Geology, v. 41, p. 27–30, https://doi.org/10.1130/G33422.1.

Kuypers, M.M., van Breugel, Y., Schouten, S., Erba, E., and Damsté, J.S.S., 2004, N_2-fixing cyanobacteria supplied nutrient N for Cretaceous oceanic anoxic events: Geology, v. 32, p. 853–856, https://doi.org/10.1130/G20458.1.

Little, S., Vance, D., Walker-Brown, C., and Landing, W., 2014, The oceanic mass balance of copper and zinc isotopes, investigated by analysis of their inputs, and outputs to ferromanganese oxide sediments: Geochimica et Cosmochimica Acta, v. 125, p. 673–693, https://doi.org/10.1016/j.gca.2013.07.046.

Little, S.H., Vance, D., McManus, J., and Severmann, S., 2016, Key role of continental margin sediments in the oceanic mass balance of Zn and Zn isotopes: Geology, v. 44, p. 207–210, https://doi.org/10.1130/G37493.1.

Liu, S.-A., Wu, H., Shen, S.-Z., Jiang, G., Zhang, S., Lv, Y., Zhang, H., and Li, S., 2017, Zinc isotope evidence for intensive magmatism immediately before the end-Permian mass extinction: Geology, v. 45, p. 343–346, https://doi.org/10.1130/G38644.1.

Marchitto, T.M., Curry, W.B., and Oppo, D.W., 2000, Zinc concentrations in benthic foraminifera reflect seawater chemistry: Paleoceanography, v. 15, p. 299–306, https://doi.org/10.1029/1999PA000420.

Monteiro, F., Pancost, R., Ridgwell, A., and Donnadieu, Y., 2012, Nutrients as the dominant control on the spread of anoxia and euxinia across the Cenomanian-Turonian oceanic anoxic event (OAE2): Model-data comparison: Paleoceanography, v. 27, p. PA4209, https://doi.org/10.1029/2012PA002351.

Mort, H.P., Adatte, T., Föllmi, K.B., Keller, G., Steinmann, P., Matera, V., Berner, Z., and Stüben, D., 2007, Phosphorus and the roles of productivity and nutrient

recycling during oceanic anoxic event 2: Geology, v. 35, p. 483–486, https://doi.org/10.1130/G23475A.1.

Owens, J.D., Gill, B. C., Jenkyns, H.C., Bates, S.M., Severmann, S., Kuypers, M. M. M., Woodfine, R. G., and Lyons, T.W., 2013, Sulfur isotopes track the global extent and dynamics of euxinia during Cretaceous Oceanic Anoxic Event 2: Proceedings of the National Academy of Sciences of the United States of America, v. 110 (46), p. 18407-18412, doi: 10.1073/pnas.1305304110.

Owens, J.D., Reinhard, C.T., Rohrssen, M., Love, G.D., and Lyons, T.W., 2016, Empirical links between trace metal cycling and marine microbial ecology during a large perturbation to Earth's carbon cycle: Earth and Planetary Science Letters, v. 449, p. 407–417, https://doi.org/10.1016/j.epsl.2016.05.046.

Parente, M., Frijia, G., Di Lucia, M., Jenkyns, H.C., Woodfine, R.G., and Baroncini, F., 2008, Stepwise extinction of larger foraminifers at the Cenomanian-Turonian boundary: A shallow-water perspective on nutrient fluctuations during Oceanic Anoxic Event 2 (Bonarelli Event): Geology, v. 36, p. 715–718, https://doi.org/10.1130/G24893A.1.

Pichat, S., Douchet, C., and Albarède, F., 2003, Zinc isotope variations in deep-sea carbonates from the eastern equatorial Pacific over the last 175 ka: Earth and Planetary Science Letters, v. 210, p. 167–178, https://doi.org/10.1016/S0012-821X(03)00106-7.

Tsikos, H., Jenkyns, H., Walsworth-Bell, B., Petrizzo, M., Forster, A., Kolonic, S., Erba, E., Silva, I.P., Baas, M., and Wagner, T., 2004, Carbon-isotope stratigraphy recorded by the Cenomanian–Turonian Oceanic Anoxic Event: Correlation and implications

based on three key localities: Journal of the Geological Society, v. 161, p. 711–719, https://doi.org/10.1144/0016-764903-077.

Turgeon, S.C., and Creaser, R.A., 2008, Cretaceous oceanic anoxic event 2 triggered by massive magmatic episode: Nature, v. 454, p. 323–326, https://doi.org/10.1038/nature07076.

Van Helmond, N.A., Sluijs, A., Papadomanolaki, N.M., Plint, A.G., Gröcke, D.R., Pearce, M.A., Eldrett, J.S., Trabucho-Alexandre, J., Walaszczyk, I., and Schootbrugge, B.d., 2016, Equatorward phytoplankton migration during a cold spell within the Late Cretaceous super-greenhouse: Biogeosciences, v. 13, p. 2859–2872, https://doi.org/10.5194/bg-13-2859-2016.

Vance, D., Little, S.H., Archer, C., Cameron, V., Andersen, M.B., Rijkenberg, M.J., and Lyons, T.W., 2016, The oceanic budgets of nickel and zinc isotopes: The importance of sulfidic environments as illustrated by the Black Sea: Philosophical Transansactions of the Royal Society A, v. 374, p. 20150294, https://doi.org/10.1098/rsta.2015.0294.

Wyatt, N.J., Milne, A., Woodward, E.M.S., Rees, A.P., Browning, T.J., Bouman, H.A., Worsfold, P.J., and Lohan, M.C., 2014, Biogeochemical cycling of dissolved zinc along the Geotraces South Atlantic transect GA10 at 40°S: Global Biogeochemical Cycles, v. 28, p. 44–56, https://doi.org/10.1002/2013GB004637.

FIGURE CAPTIONS

Figure 1. Schematic representation of Zn-isotope systematics based on data compiled by Little et al. (2014, 2016) and Vance et al. (2016). The sizes of the circles represent relative flux sizes, the numbers their isotopic composition in ‰. The diagrams indicate end-member steady-state oceanographic conditions.

Figure 2. Paleogeographical reconstruction for the Cenomanian–Turonian boundary interval, modified from Owens et al. (2013) with approximate sample locations.

Figure 3. Zn-isotope ($\delta^{66}Zn$) stratigraphy of Cenomanian–Turonian carbonates. The Raia del Pedale and Barranca el Cañón data were converted to the Eastbourne depth scale by tying key inflection points from the published carbon-isotope stratigraphies available for each location (Tsikos et al., 2004; Parente et al., 2008; Elrick et al. 2009, SI). Chalk intervals are shown as blank, marls as stippled (Tsikos et al., 2004). A and B highlight decreases toward lower $\delta^{66}Zn$ values. The horizontal black line marks the extinction level of larger foraminifera as recorded in the Raia del Pedale section (Parente et al., 2008). The vertical orange band represents the time interval associated with unradiogenic Os-isotope seawater compositions in the global ocean (Jenkyns et al., 2017).

1GSA Data Repository item 2018xxx, xxxxxxxx, is available online at http://www.geosociety.org/datarepository/2018/ or on request from editing@geosociety.org.

Isotopically light deep ocean

- High volcanic/hydrothermal input
- Light Zn remobilized from continental margin sediments
- Sparse organic-rich continental margin sinks for isotopically light Zn
- Abundant oxic sinks for isotopically heavy Zn

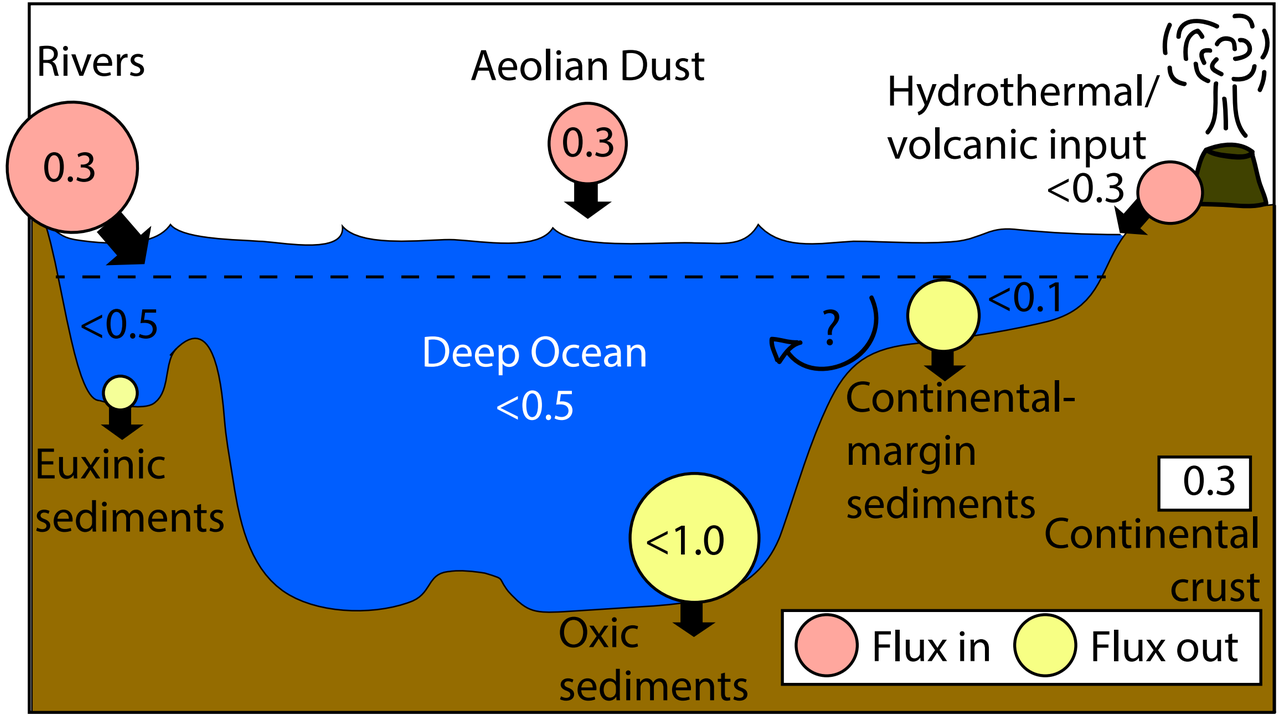

Isotopically heavy deep ocean

- Low volcanic/hydrothermal input
- Mostly organic-rich continental margin sinks for isotopically light Zn
- Sparse oxic sinks for isotopically heavy Zn

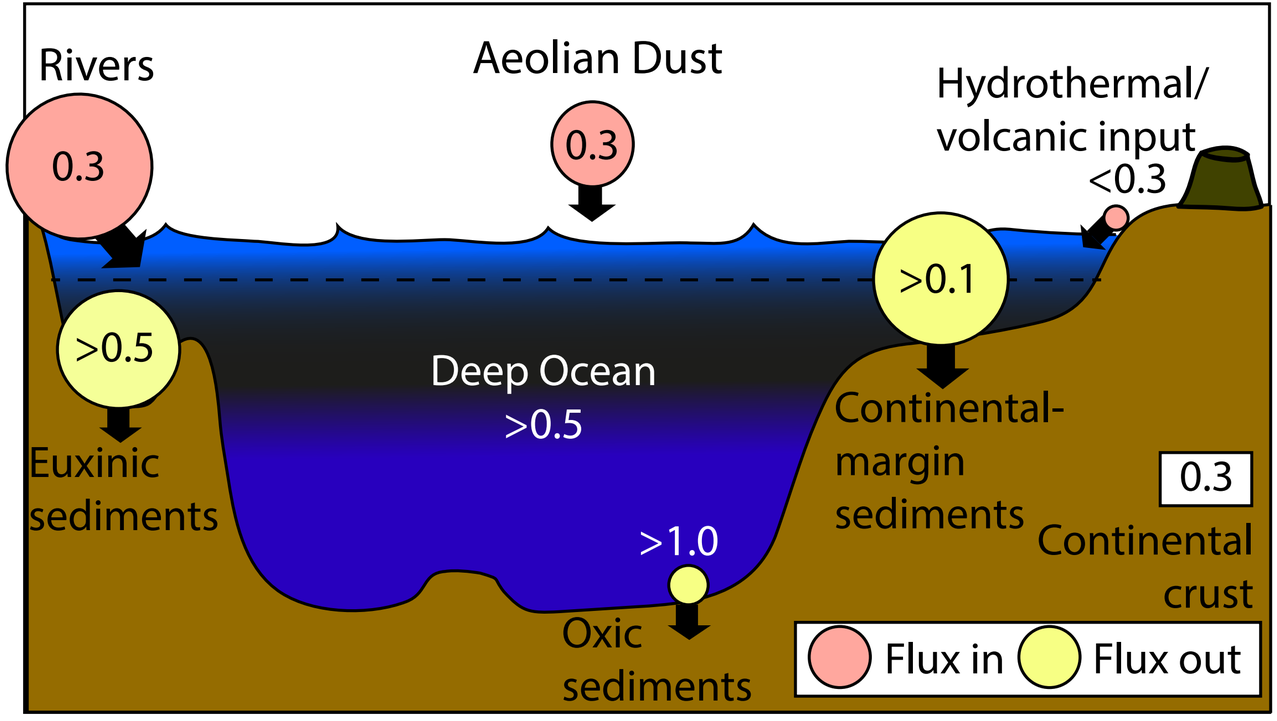

Figure 2

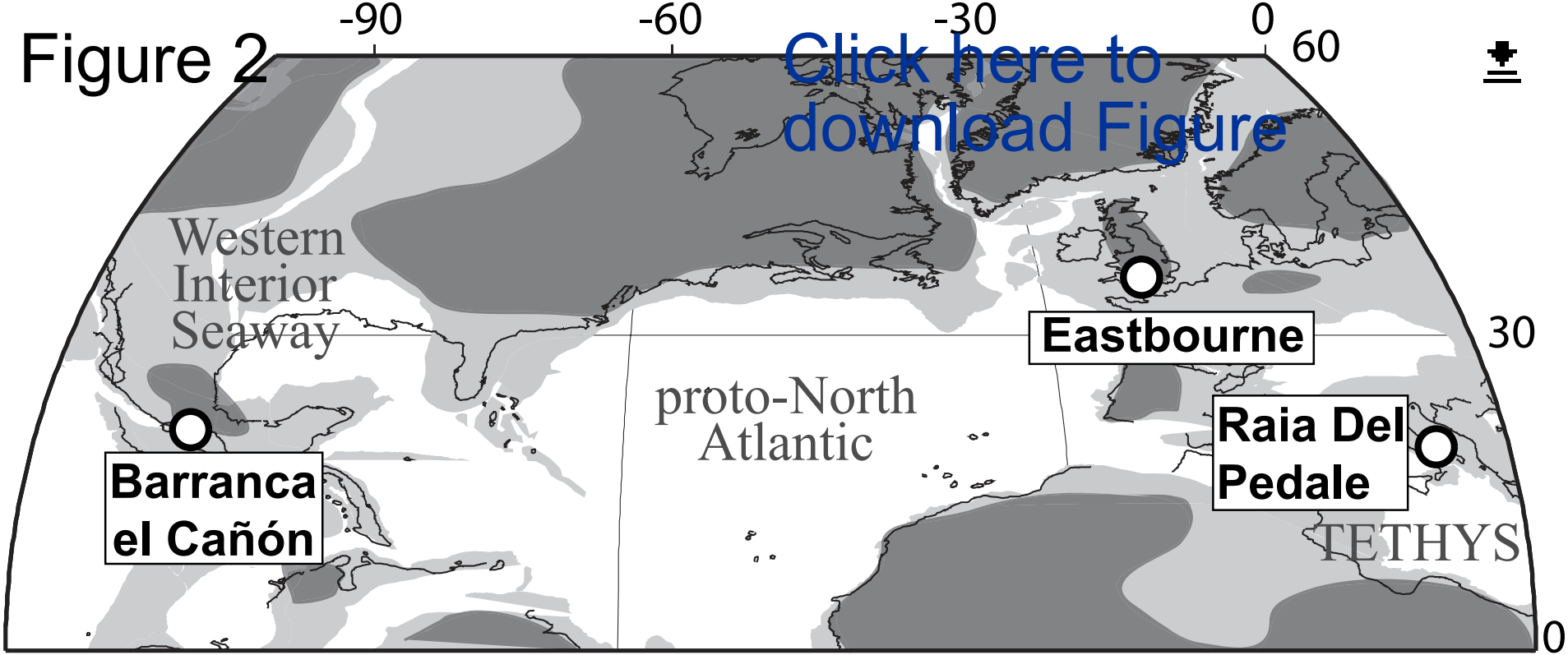

Click here to download Figure

Figure 3

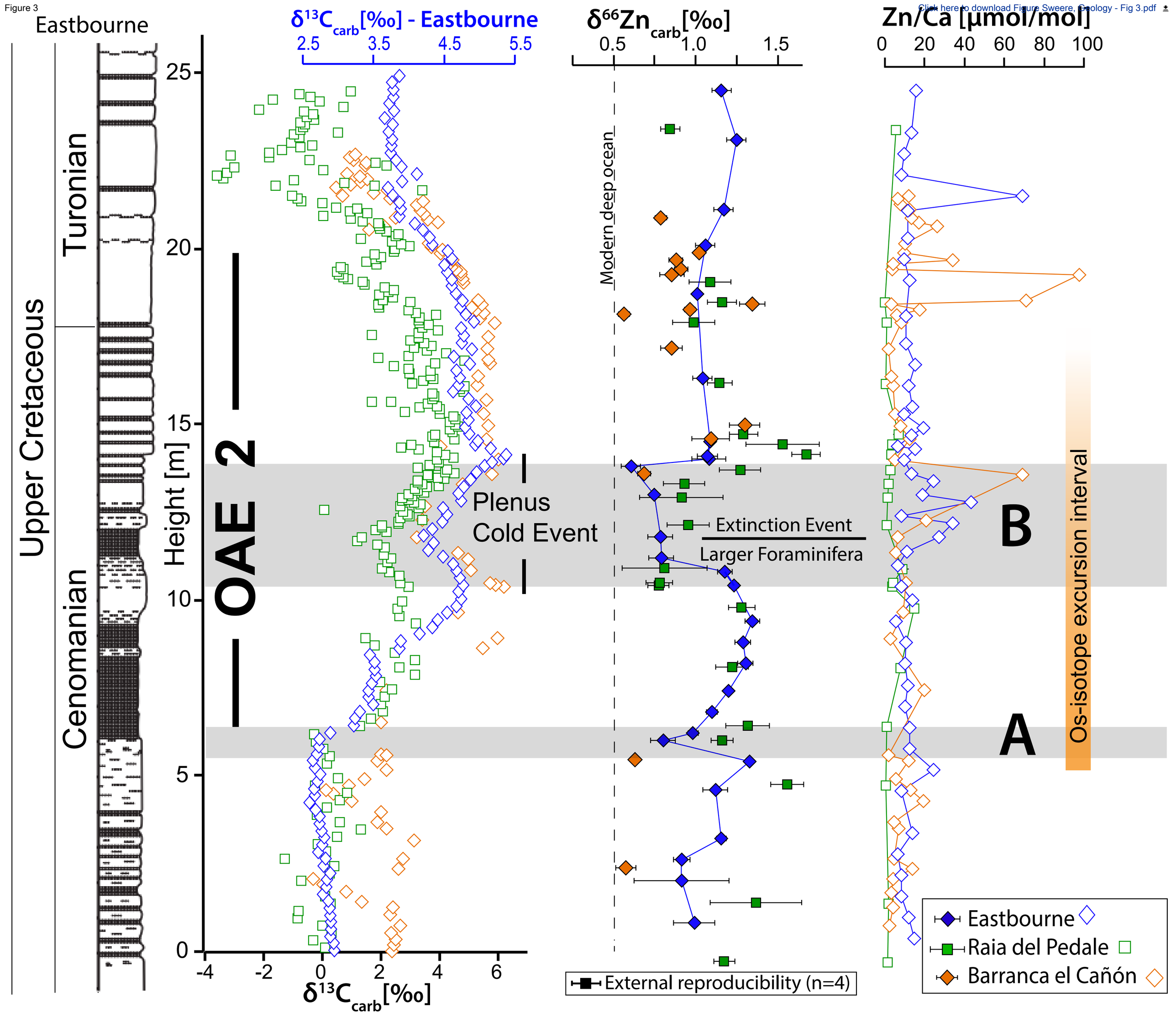

SUPPLEMENTARY INFORMATION

Isotopic evidence for changes in the zinc cycle during Oceanic Anoxic Event 2 (Late Cretaceous) – Sweere et al.

Analytical methods - $\delta^{66}Zn$

Samples were selected based on visual inspection and available data (e.g. %TOC, % insoluble, elemental abundances) to minimize contribution from any non-carbonate sources of Zn. A leaching procedure similar to previously established methods was used to preferentially dissolve the carbonate fraction for these samples (Pichat et al., 2003, Kunzmann et al., 2013, Liu et al., 2017). 0.5–1 g of crushed material was treated with KCl and then rinsed and sonicated in Milli-Q ultrapure water to remove the exchangeable fraction (Tessier et al., 1979). The carbonate phase was selectively dissolved using 0.5M acetic acid, which was added slowly in 0.5 ml aliquots to allow the dissolving carbonate to act as a pH buffer. After centrifugation to remove undissolved phases, an aliquot of the supernatant was analyzed for Zn abundances on a ThermoFisher ELEMENT 2 ICP-MS or, using isotope dilution, on a MC-ICP-MS at the University of Oxford. Another aliquot was then spiked with a ^{67}Zn-^{64}Zn double spike to obtain a spike:sample ratio of ~1.4 (Rudge et al., 2009).

Zn was separated using AG1X-8 anion exchange resin (200–400 mesh) loaded onto shrink-fit Teflon columns with a resin bed of 200 µL. Samples were loaded in 0.6 ml 1M HF / 0.5M HCl, and major-element cations and isobaric interferences (Ni and Ba) were subsequently eluted with a further 1.5 ml 1M HF / 0.5M HCl, followed by 1.5 ml of 4M HCl. Zn was then eluted with 2.2ml 0.5M HF. The column procedure was repeated to ensure maximum removal of Ni and Ba from the sample matrix. All chemistry was done in Teflon using distilled acids.

Stable-isotope measurements were performed using a Nu Plasma MC-ICP-MS in medium-resolution mode, on 120 ppb (spike plus sample) Zn solutions. Zn-isotope

compositions were measured relative to the IRMM 3702 standard (Moeller et al., 2012) and then expressed relative to AA-ETH Zürich Zn +0.28 ‰, as suggested by Archer et al. (2017), as AA-ETH Zürich Zn and IRMM 3702 are isotopically indistinguishable.

$$\delta^{66}Zn = \left(\frac{^{66}Zn/^{64}Zn_{sample} - {}^{66}Zn/^{64}Zn_{IRMM}}{^{66}Zn/^{64}Zn_{IRMM}}\right) * 1000 + 0.28\ ‰$$

Error bars represent the propagated uncertainties based on 2 standard errors of the counting statistics and reproducibility of bracketing standards. External reproducibility was estimated by analysis of reference material BCS-CRM 393 (ECRM 752-1) with a $\delta^{66}Zn$ composition of 0.75 ± 0.09 **‰** (2 SD, n = 4) and secondary isotope standard 'London Zn' with a $\delta^{66}Zn$ of 0.09 ± 0.08 **‰** (2 SD, n = 19), which is in agreement with published values (Moeller et al., 2012). Procedural blanks were determined for every batch using isotope dilution and were always <2 ng (n = 9), which is <1 % of all Zn processed.

Analytical methods - Zn/Ca

Sample preparation for Zn/Ca and Zn/Al analyses were largely similar to the method outlined above for the Zn-isotope analysis, with exclusion of the first KCl stage to remove the exchangeable fraction. Elemental abundances were analyzed on a ThermoFisher ELEMENT 2 ICP-MS at the University of Oxford. For some samples (Raia del Pedale), Zn abundances were below detection limit using ICP-MS analysis so Zn/Ca values for this site were measured by isotope dilution by MC-ICP-MS. Where Ca concentration data were not available on the same sample aliquot for these samples, Ca was estimated using the sample weight before leaching and assuming a

Ca concentration of 40% in the leachable fraction. These samples were given an estimated error bar (of 40%) relative to the Zn/Ca ratio associated with this estimate.

Contribution of Zn from detrital minerals

Pelagic and platform carbonates are expected to record Zn-isotope values in the upper part of the water column. However, the high abundance of Zn in detrital minerals means that liberation of Zn from non-carbonate phases during chemical preparation may obscure these primary trends. Zn/Al ratios can be used to estimate the proportion of Zn leached from detrital minerals relative to total leached Zn, where Al is taken to represent the amount of leaching from detrital minerals.

Zn/Al ratios were measured by ThermoFisher ELEMENT 2 ICP-MS at the University of Oxford during the same analysis as the Zn/Ca measurements, and are therefore for samples leached without KCl treatment to remove the exchangeable fraction. This leach therefore differs slightly from that used for the Zn-isotope samples, but the amount of Zn in the exchangeable fraction is very low (Tessier et al., 1979) so this small difference in leaching methods is not expected to influence significantly the estimated proportion of Zn associated with detrital minerals. Stratigraphic Zn/Al patterns do not show signs of increased leaching from detrital minerals (i.e. drops to lower Zn/Al values) during intervals of lithological or δ^{66}Zn change, which suggests the leaching of Zn from detrital minerals does not impact stratigraphic δ^{66}Zn patterns (Figure 1).

If leaching of Zn and Al from detrital minerals is assumed to be proportional, these abundances can be used to estimate the amount of zinc liberated from the lithogenic component as a fraction of total leached zinc using:

$$X_{lith} = [(Zn/Al)_{lith} / (Zn/Al)_{carb}] * 100\ \%$$

with X_{lith} being the lithogenic (detrital) fraction of Zn in the leachate, $(Zn/Al)_{lith}$ based on the average composition of upper continental crust (Rudnick and Gao, 2003), and $(Zn/Al)_{carb}$ the measured concentrations in the leachate. Following this approach, the maximum X_{lith} found are 0.13 and 0.51 % for Eastbourne and Barranca el Cañón sections, respectively. Given this low detrital component, no attempt to correct carbonate $\delta^{66}Zn$ values for detrital input was made.

Contribution of Zn from ferromanganese coatings

Like previous Zn-isotope studies on carbonates (Pichat et al., 2003, Kunzmann et al., 2013, Liu et al., 2017), the applied method for the selective dissolution of the carbonate fraction does not include a reductive cleaning step prior to the dissolution of carbonate minerals. Such techniques are used in other studies to remove potential contamination from ferromanganese coatings (e.g. Clarkson et al., 2018). The exclusion of this cleaning procedure allows better comparison to previously published Zn-isotope data from carbonates, but does mean there is potential for contamination. In ferromanganese crusts, Zn is relatively abundant and isotopically heavier (~+0.5‰) than deep-ocean compositions (Little et al., 2014a). Zn in ferromanganese crusts is predominantly associated with birnessite (δ-MnO_2), so Mn abundances of the leachates may be used to address possible contamination (Little et al., 2014b). These data imply that Zn derived from ferromanganese coatings does not have a significant impact on the Zn/Ca and $\delta^{66}Zn$ data presented here.

Firstly, Mn/Ca values found for the leachates in this study are comparable to those presented by Clarkson et al. (2018) who present Mn/Ca on the same Raia del Pedale and Eastbourne sample sets and do include a reductive cleaning step prior to carbonate dissolution. Their data imply that the large majority of Mn (and by

inference Zn) present in the leachates from this study is associated with the carbonate phase rather than derived from ferromanganese coatings.

Secondly, stratigraphic Mn/Ca patterns vary independently of δ^{66}Zn and Zn/Ca, and stratigraphic Zn/Ca patterns are comparable to Zn/Mn data (Figure 2). Together, these observations suggest that varying contributions of Zn from ferromanganese coatings do not dominate stratigraphic patterns.

Finally, the lowest Zn/Mn values found are ~0.0052 and 0.0088 mol/mol for the Eastbourne and Barranca el Canon sections, respectively, which is higher than the ~0.0025 mol/mol found for average ferromanganese crusts (Little et al., 2014a). Assuming average ferromanganese crust composition for ferromanganese coatings in these carbonates, this suggests that, if all Mn in the leachates were derived from ferromanganese coatings, a maximum of 48% of total Zn would be derived from ferromanganese coatings. However, comparison with the Clarkson et al. (2018) data implies that most Mn is actually in the carbonate phase. The maximum proportion of Zn in the leachates presented here therefore is likely substantially lower than 48%. Additionally, Zn/Ca ratios in reductively cleaned foraminifera are comparable to or higher than values found for the carbonates in this study (Boyle, 1981).

FIGURE CAPTIONS

Figure 1 Zn/Al ratios, used to assess the amount of zinc leached from detrital phases. See text for discussion.

Figure 2 Mn/Ca ratios for the different sites. See text for discussion.

Figure 3 Stratigraphic correlation of the three sections based on tying key inflection points from the published high-resolution carbon-isotope stratigraphies available for each location (Tsikos et al., 2004; Parente et al., 2008; Elrick et al 2009).

REFERENCES CITED

Archer, C., et al., 2017, Inter-calibration of a proposed new primary reference standard AA-ETH Zn for zinc isotopic analysis: Journal of Analytical Atomic Spectrometry, v. 32, p. 415–419, doi:10.1039/c6ja00282j.

Clarkson, M. O., Stirling, C. H., Jenkyns, H. C., Dickson, A. J., Porcelli, D., Moy, C. M., Pogge von Strandmann, P. A. E., Cooke, I. R, and Lenton, T. M., 2018, Uranium isotope evidence for two episodes of deoxygenation during Oceanic Anoxic Event 2: Proceedings of the National Academy of Sciences.

Elrick, M., Molina-Garza, R., Duncan, R., and Snow, L., 2009, C-isotope stratigraphy and paleoenvironmental changes across OAE2 (mid-Cretaceous) from shallow-water platform carbonates of southern Mexico: Earth and Planetary Science Letters, v. 277, p. 295–306, doi:10.1016/j.epsl.2008.10.020.

Kunzmann, M., Halverson, G. P., Sossi, P. A., Raub, T. D., Payne, J. L., and Kirby, J., 2013, Zn isotope evidence for immediate resumption of primary productivity after snowball Earth: Geology, v. 41, p. 27–30, doi:10.1130/G33422.1.

Liu, S.-A., Wu, H., Shen, S.-Z., Jiang, G., Zhang, S., Lv, Y., Zhang, H., and Li, S., 2017, Zinc isotope evidence for intensive magmatism immediately before the end-Permian mass extinction: Geology, v. 45, p. 343–346, doi:10.1130/G38644.1.

Little, S., Vance, D., Walker-Brown, C., and Landing, W., 2014a, The oceanic mass balance of copper and zinc isotopes, investigated by analysis of their inputs, and outputs to ferromanganese oxide sediments: Geochimica et Cosmochimica Acta, v. 125, p. 673–693, doi:10.1016/j.gca.2013.07.046.

Little, S., Sherman, D.M., Vance, D., and Hein, J.R., 2014b, Molecular controls on Cu and Zn isotopic fractionation in Fe–Mn crusts: Earth and Planetary Science Letters, v. 396, p 213–222.

Moeller, K., Schoenberg, R., Pedersen, R. B., Weiss, D., and Dong, S., 2012, Calibration of the New Certified Reference Materials ERM-AE633 and ERM-AE647 for Copper and IRMM-3702 for Zinc Isotope Amount Ratio Determinations: Geostandards and Geoanalytical Research, v. 36, p. 177–199, doi:10.1111/j.1751-908X.2011.00153.x.

Parente, M., Frijia, G., Di Lucia, M., Jenkyns, H. C., Woodfine, R. G., and Baroncini, F., 2008, Stepwise extinction of larger foraminifers at the Cenomanian-Turonian boundary: A shallow-water perspective on nutrient fluctuations during Oceanic Anoxic Event 2 (Bonarelli Event): Geology, v. 36, p. 715–718, doi: 10.1130/G24893A.1.

Pichat, S., Douchet, C., and Albarède, F., 2003, Zinc isotope variations in deep-sea carbonates from the eastern equatorial Pacific over the last 175 ka: Earth and Planetary Science Letters, v. 210, p. 167–178, doi:10.1016/S0012-821X(03)00106-7.

Rudge, J. F., Reynolds, B. C., and Bourdon, B., 2009, The double spike toolbox: Chemical Geology, v. 265, p. 420–431, doi:10.1016/j.chemgeo.2009.05.010.

Rudnick, R.L., and Gao, S., 2003, Composition of the continental crust:, Treatise on Geochemistry, v. 3, p. 1–64, doi: 10.1016/B0-08-043751-6/03016-4.

Tessier, A., Campbell, P. G., and Bisson, M., 1979, Sequential extraction procedure for the speciation of particulate trace metals: Analytical Chemistry, v. 51, p. 844–851.

Tsikos, H., Jenkyns, H., Walsworth-Bell, B., Petrizzo, M., Forster, A., Kolonic, S., Erba, E., Silva, I. P., Baas, M., and Wagner, T., 2004, Carbon-isotope stratigraphy recorded by the Cenomanian–Turonian Oceanic Anoxic Event: correlation and implications based on three key localities: Journal of the Geological Society, v. 161, p. 711–719, doi:10.1144/0016-764903-077.

Eastbourne

Upper Cretaceous

Turonian

Cenomanian

Height [m]

$\delta^{13}C_{carb}$ [‰] - Eastbourne

$\delta^{13}C_{carb}$ [‰]

OAE 2

Plenus Cold Event

$\delta^{66}Zn_{carb}$ [‰]

Modern deep ocean

Zn/Al crust

Extinction Event

Larger Foraminifera

Eastbourne

Raia del Pedale

Barranca el Cañón

External reproducibility (n=4)

Zn/Al leach Eastbourne

Zn/Al leach Barranca el Canon

0.13% detrital

0.51% detrital

Zn/Al crust

Zn/Al

A

B

SI Figure 2

Click here to download Figure SI, geology Fig 2 - Mn.pdf

Eastbourne

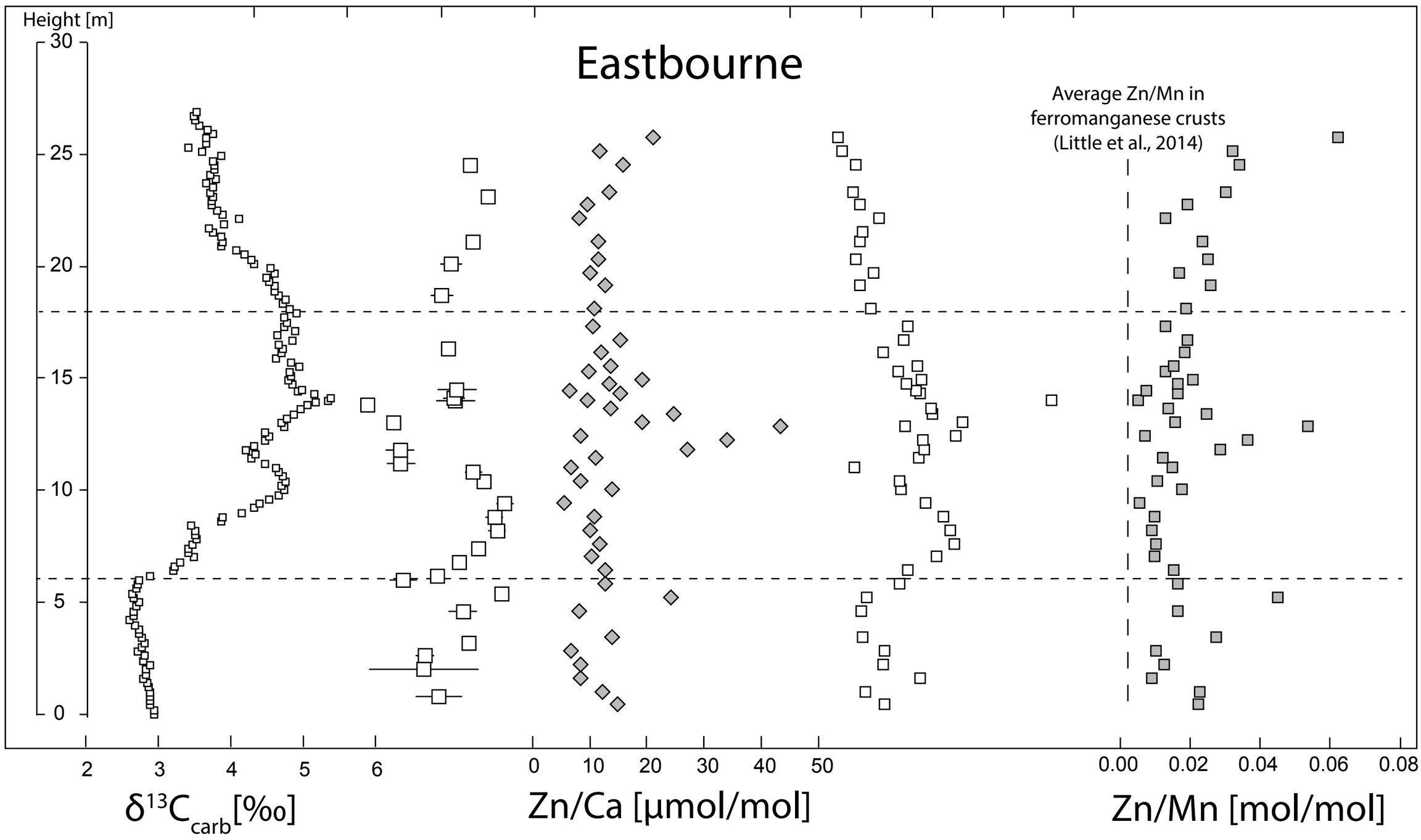

Barranca el Cañón

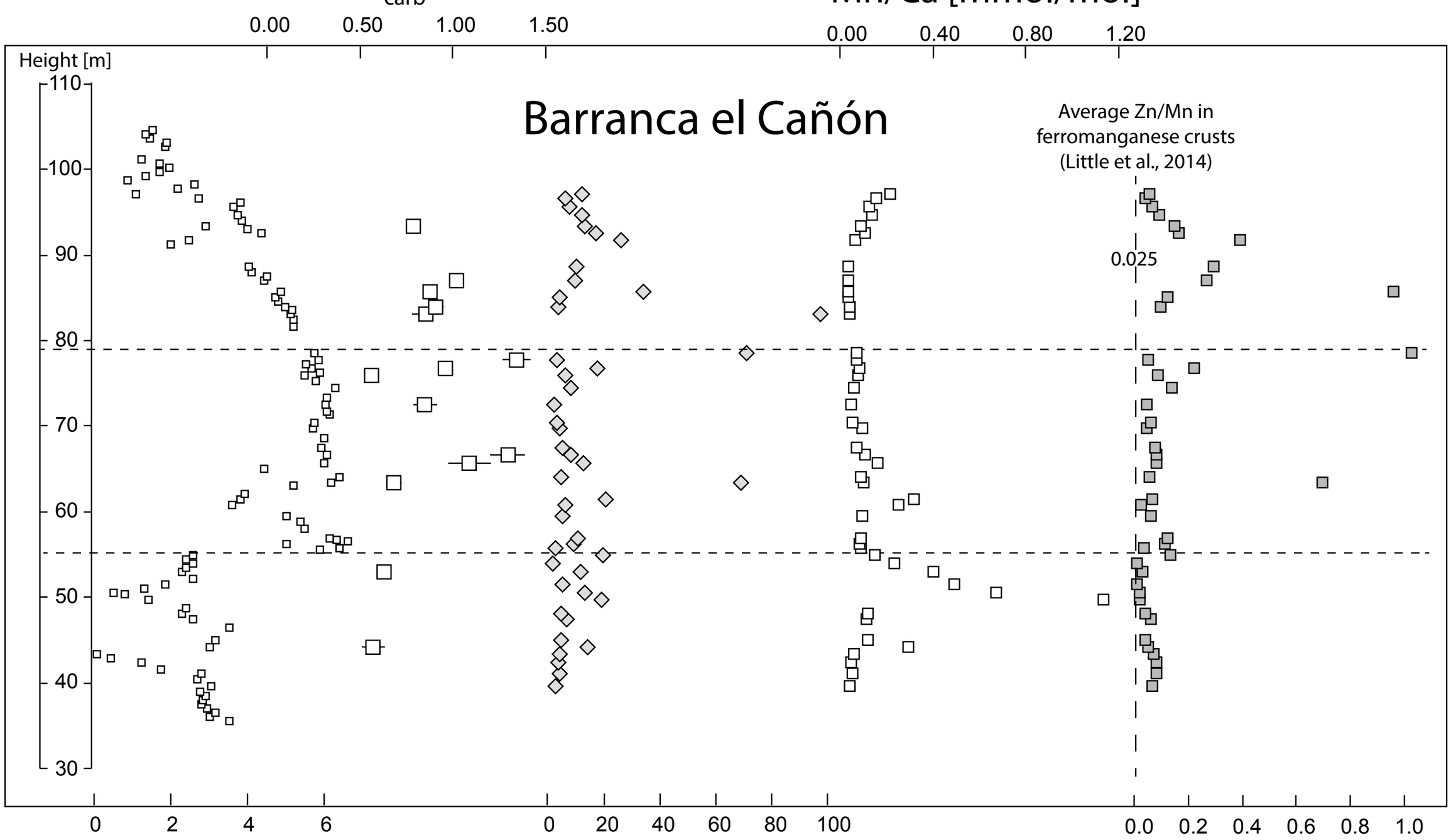

Raia del Pedale

SI Figure 3

Click here to download Figure SI, geology Fig 3 - strat correlationv2.pdf

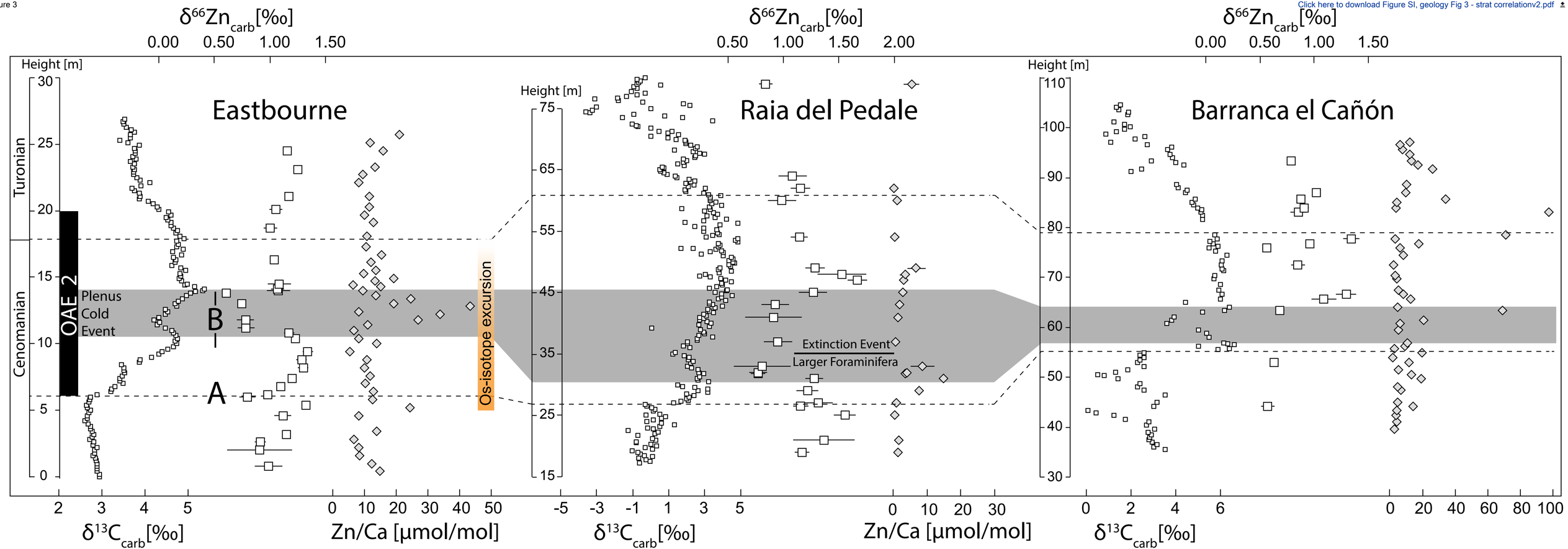

Supplemental data

Click here to download Supplemental file Sweere et al., Geology - SI data.xlsx

Eastbourne		
Height [m]	d66/64 Zn	2 s.e.
0.8	0.99	0.13
2	0.91	0.29
2.6	0.91	0.05
3.2	1.15	0.03
4.6	1.12	0.08
5.4	1.32	0.01
6	0.80	0.07
6.2	0.98	0.03
6.8	1.10	0.03
7.4	1.20	0.01
8.2	1.30	0.05
8.8	1.28	0.05
9.4	1.34	0.05
10.4	1.23	0.03
10.8	1.17	0.05
11.2	0.79	0.08
11.8	0.78	0.08
13	0.74	0.02
13.8	0.61	0.02
14	1.08	0.10
14.1	1.07	0.06
14.5	1.09	0.10
16.3	1.04	0.00
18.7	1.01	0.06
20.1	1.05	0.06
21.1	1.17	0.00
23.1	1.25	0.00
24.5	1.15	0.00

BC (Mexico)			
Height [m]	Eastbourne height equivalent	d66/64 Zn	2 s.e.
44.2	2.37	0.57	0.06
53	5.45	0.63	0.03
63.4	13.59	0.68	0.04
65.6	14.59	1.09	0.12
66.6	14.97	1.29	0.09
72.5	17.16	0.85	0.07
75.9	18.12	0.56	0.03
76.8	18.26	0.96	0.03
77.8	18.42	1.34	0.08
83.1	19.26	0.85	0.08
84	19.41	0.91	0.04
85.7	19.68	0.88	0.04
87	19.88	1.02	0.03
93.3	20.88	0.78	0.04

Raia del Pedale

Height [m]	Eastbourne height equivalent	d66/64 Zn	2 s.e.
19	-0.29	1.17	0.06
21	1.39	1.36	0.28
25	4.74	1.55	0.10
26.5	6.00	1.16	0.07
27	6.42	1.31	0.13
29	8.10	1.22	0.10
31	9.77	1.28	0.08
31.75	10.40	0.77	0.07
32	10.50	0.78	0.08
33	10.90	0.81	0.26
37	12.14	0.95	0.13
41	12.92	0.91	0.26
43	13.32	0.93	0.13
45	13.71	1.27	0.13
47	14.14	1.67	0.09
48	14.43	1.53	0.22
49	14.72	1.29	0.09
54	16.17	1.14	0.08
60	17.90	0.99	0.13
62	18.48	1.16	0.09
64	19.06	1.08	0.13
79	23.39	0.84	0.06

Eastbourne			
Height [m]	Zn/Ca [umol/mol]	Al/Ca [umol/mol]	Mn/Ca [mmol/mol]
0.40	14.87	6.95	0.6665
1.00	12.30	4.67	0.5364
1.60	8.44	8.47	0.9134
2.20	8.36	5.78	0.6599
2.80	6.79	7.86	0.6697
3.40	13.95	8.43	0.5085
4.60	8.31	8.57	0.5049
5.20	24.32	13.97	0.5387
5.80	12.77	17.30	0.7749
6.40	12.78	13.39	0.8329
7.00	10.23	20.94	1.0344
7.60	11.80	15.84	1.1541
8.20	10.21	24.56	1.1302
8.80	10.77	20.40	1.0850
9.40	5.49	21.29	0.9526
10.00	13.82	10.12	0.7818
10.40	8.36	11.30	0.7743
11.00	6.73	4.32	0.4525
11.40	11.02	18.62	0.9125
11.80	27.09	14.58	0.9430
12.20	33.99	14.47	0.9386
12.40	8.32	5.71	1.1670
12.80	43.40	42.81	0.8125
13.00	19.20	8.50	1.2194
13.40	24.65	13.35	1.0012
13.60	13.68	8.36	0.9951
14.00	9.63	4.79	1.8404
14.30	15.26	4.96	0.9173
14.40	6.57	8.57	0.8904
14.70	13.45	4.07	0.8217
14.90	19.29	5.96	0.9257
15.30	9.78	4.68	0.7612
15.50	13.78	5.21	0.8979
16.10	12.08	5.39	0.6568
16.70	15.41	4.71	0.8041
17.30	10.62	5.09	0.8274
18.10	10.79	4.25	0.5690
19.10	12.78	3.14	0.4962
19.70	9.99	3.17	0.5947
20.30	11.66	5.38	0.4630
21.10	11.59	6.58	0.4950
21.50	68.82	36.78	0.5139
22.10	8.21	8.32	0.6258
22.70	9.65	5.31	0.4968
23.30	13.37	4.94	0.4428
24.50	15.94	7.63	0.4679
25.10	11.82	4.95	0.3680
25.70	21.18	8.67	0.3400

BC (	
Height [m]	Eastbourne height equivalent [m]
39.60	0.76
41.10	1.29
42.30	1.71
43.40	2.09
44.20	2.37
45.00	2.65
47.50	3.53
48.00	3.70
49.70	4.30
50.60	4.61
51.50	4.93
53.00	5.45
54.00	5.60
55.00	7.45
55.80	8.92
56.20	9.66
56.90	10.50
59.50	11.37
60.80	11.80
61.50	12.28
63.40	13.59
64.00	14.00
65.60	14.59
66.60	14.97
67.50	15.30
69.70	16.12
70.40	16.38
72.50	17.16
74.50	17.90
75.90	18.12
76.80	18.26
77.80	18.42
78.50	18.53
83.10	19.26
84.00	19.41
85.00	19.57
85.70	19.68
87.00	19.88
88.70	20.15
91.80	20.64
92.50	20.75
93.30	20.88
94.70	21.10
95.70	21.26
96.70	21.42
97.20	21.50

Mexico)

Zn/Ca [umol/mol]	Al/Ca [umol/mol]	ı/Ca [mmol/mol]
2.59	2.86	0.04
4.42	2.83	0.05
3.61	3.29	0.04
4.23	3.15	0.06
14.12	90.75	0.30
4.90	25.15	0.12
7.02	9.52	0.11
4.70	6.23	0.12
19.22	294.51	1.14
13.23	134.50	0.67
5.50	26.95	0.49
11.93	33.94	0.40
2.04	5.89	0.23
19.89	6.30	0.15
3.02	27.87	0.09
9.41	26.64	0.08
10.83	26.74	0.09
5.55	2.68	0.10
6.49	23.25	0.25
20.98	33.21	0.32
68.97	6.17	0.10
4.99	3.42	0.09
12.71	15.20	0.16
8.18	10.29	0.10
5.30	5.71	0.07
4.31	8.74	0.10
3.30	9.97	0.05
2.16	2.23	0.05
8.28	3.39	0.06
6.37	5.73	0.08
17.84	32.47	0.08
3.41	4.99	0.07
70.99	14.32	0.07
97.39	8.42	0.04
3.72	3.66	0.04
4.53	3.60	0.04
34.15	3.97	0.04
9.83	3.47	0.04
10.23	2.15	0.04
26.22	58.87	0.07
17.14	6.97	0.10
13.45	24.15	0.09
12.37	5.38	0.14
7.91	6.82	0.12
6.47	3.93	0.16
12.08	69.56	0.21

Raia del Pedale

Height [m]	Eastbourne height equivalent [m]	Zn [umol/mol]	2 s.e.
19.00	-0.29	1.51	0.60
21.00	1.39	1.79	
25.00	4.74	0.53	0.21
27.00	6.42	1.04	0.42
29.00	8.10	7.75	
31.00	9.77	14.81	
31.75	10.40	3.75	
32.00	10.50	4.11	
33.00	10.90	8.67	3.47
37.00	12.14	0.88	0.35
41.00	12.92	1.39	0.56
43.00	13.32	1.92	0.77
45.00	13.71	3.02	1.21
47.00	14.14	3.17	1.27
48.00	14.43	3.64	
49.00	14.72	6.86	2.75
54.00	16.17	0.47	0.19
60.00	17.90	1.24	0.50
62.00	18.48	0.36	0.15
79.00	23.39	5.64	2.26

Height (m)	Mn/ca [mmol/mol]
19	0.028577386
20.25	0.014308717
21	0.011048051
23	0.015998819
25	0.013119209
26.5	0.011710924
26.5	0.011803042
26.75	0.011869314
27	0.017747641
29	0.009552367
31	0.01108791
33	0.012132457
35	0.013984213
37	0.014528182
39	0.019061035
41	0.023178392
43	0.019874931
45	0.00963873
47	0.010578457
48	0.011029387
49	0.010295044
51	0.01049557
52	0.010151806
54	0.008945039
55	0.018921778
57	0.009860267
58	0.009732214
60	0.010634712
61	0.013067966
62	0.011920156
63	0.012504713
64	0.014502171
66	0.018056854
68	0.0109351
70	0.019450218
71	0.025798882
72	0.011660729
74	0.023363286
75	0.015561623
77	0.028921983
79	0.033060769
80	0.03402227